Nuclear Materials and Energy 41 (2024) 101766

Contents lists available at ScienceDirect

Nuclear Materials and Energy

journal homepage: www.elsevier.com/locate/nme

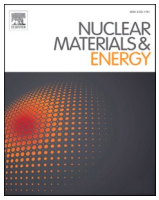

Divertor erosion at ASDEX Upgrade during helium plasma operations

Tomi Vuoriheimo [a,*], Antti Hakola [b], Jari Likonen [b], Karl Krieger [c], Martin Balden [c], Iva Bogdanović Radović [d], Georgios Provatas [d], Zdravko Siketić [d], Karla Ivanković Nizić [d], Marcin Rasinski [e], Sebastijan Brezinsek [e], ASDEX Upgrade Team[1], the EUROfusion Tokamak Exploitation Team[2]

[a] Department of Physics, University of Helsinki, Helsinki, Finland
[b] VTT, Espoo, Finland
[c] Max-Planck-Institut für Plasmaphysik, Garching, Germany
[d] Ruđer Bošković Institute, Zagreb, Croatia
[e] Forschungszentrum Jülich GmbH, Jülich, Germany

ARTICLE INFO

Keywords:
Erosion
Material migration
ASDEX Upgrade
Marker samples
Helium plasma

ABSTRACT

The effect of helium plasma operation on the erosion of plasma-facing components at the low-field side divertor of ASDEX Upgrade was investigated during the 2022 helium experimental campaign. A set of tungsten-covered graphite samples with small platinum marker spots was exposed to both L-mode and H-mode plasma discharges. The highest net erosion of over 1.1 nm/s was observed around the H-mode strike point similar to the case in deuterium plasma. Significant helium inventories of about 6×10^{16} He/cm^2 were measured in the scrape-off layer region of the divertor. Impurity deposition including boron and deuterium showed a distinct peak up to 2.4×10^{17} B/cm^2 and 1.0×10^{16} D/cm^2 between the strike points, and significant boron inventories up to 5.9×10^{16} B/cm^2 were also measured on the scrape-off layer side of the H-mode strike point. Platinum re-deposition was not detected between the marker spots, suggesting that it occurs only very locally within the markers. Overall erosion was, as expected, higher than in deuterium discharges, and it also remained comparatively high towards the scrape-off layer, unlike with deuterium.

1. Introduction

Plasma Facing Materials (PFMs) in fusion reactors are exposed to high particle and heat loads during reactor operation. It is therefore essential to understand their behavior under these conditions in order to assess their durability and their tritium (T) retention properties. The main candidate material for the reactor walls is tungsten (W), which has been selected as the PFM for the ITER divertor [1] and is going to replace beryllium as the first wall material [2]. W is also likely going to be used for DEMO [3] and widely in other future devices as well. Several fusion devices are therefore investigating the properties of W under fusion conditions, including JET [4], WEST [5], EAST [6,7], and ASDEX Upgrade (AUG) [8].

Helium (He) exposure of PFMs can occur in pure He plasmas used during the non-nuclear commissioning phase of a reactor, and also by the He ions produced in deuterium–tritium (D-T) fusion plasmas. Erosion in He plasma discharges has not been studied as extensively as for hydrogenic plasmas, but several experiments have addressed changes in surface morphology and the formation of nanoscale features (W-fuzz) by He plasma exposure [9–11]. As part of an AUG He plasma experimental campaign in 2022 to further investigate the properties of He plasmas, the effect of He on W PFM was investigated in a series of dedicated L-mode and H-mode discharges, including detailed comparisons with the available data in D [12–14]. He-induced W erosion and local redeposition and W morphology changes were quantified by exposing samples with platinum (Pt)-covered spots to He plasma to distinguish surface erosion from the intrinsic W impurity fraction. The Pt therefore functions as a proxy material for W. The samples were embedded in two custom target tiles using the DIM-II divertor manipulator [15] on the outer divertor, followed by detailed ex-situ analysis of

* Corresponding author.
E-mail address: tomi.vuoriheimo@helsinki.fi (T. Vuoriheimo).
[1] See author list of H. Zohm et al, 2024 Nucl. Fusion https://doi.org/10.1088/1741-4326/ad249d.
[2] See author list of E. Joffrin et al, 2024 Nucl. Fusion https://doi.org/10.1088/1741-4326/ad2be4.

https://doi.org/10.1016/j.nme.2024.101766
Received 5 July 2024; Received in revised form 30 September 2024; Accepted 8 October 2024
Available online 14 October 2024

the retrieved samples.

2. Experimental details

2.1. Samples used in the experiments

A total of 12 W-coated (thickness ~ 400 nm) graphite marker samples, embedded in a custom W-target tile, were prepared for exposure with DIM-II. The second tile on the DIM-II probe head was equipped with bulk W samples with pre-exposure fuzz and nanoscale features created in the PSI-2 linear plasma device and a set of polished W samples; the analyses of these samples are discussed elsewhere [16,17]. Each marker sample had a surface area of 33.5 × 12 mm^2 with either three 1 × 1 mm^2 or two 5 × 5 mm^2 evenly spaced Pt spots (thickness 40–50 nm) deposited on the W layer in a magnetron sputtering device. Both the 1 × 1 mm^2 and 5 × 5 mm^2 markers were arranged to cover a full poloidal row as shown after the exposure in Fig. 1. The samples before the exposure can be seen in ref. [17]. The 1 × 1 mm^2 markers were intended to quantify the gross erosion of the marker material, while the larger 5 × 5 mm^2 spots were used to study the net erosion behavior, as the ionization length of a few mm for Pt in the divertor plasma was expected to result in prompt gyro-orbit redeposition of a large fraction of the primarily sputtered Pt back onto the marker area. In this paper, we will concentrate on the erosion and deposition profiles of the Pt marker samples and compare the data with those from the two other sample sets.

2.2. Experiments at ASDEX Upgrade

After their exposure to the successive series of L-mode and H-mode discharges in a dedicated session, the sample tiles were immediately retrieved from the vessel to avoid distortion of the exposure effects by subsequent plasma operation. Both the L- and H-mode discharges with identical plasma current (I_p = 0.8 MA) and toroidal magnetic field (B_t = 2.5 T) were executed with a long flat-top phase of 6–7 s duration. The cross section of AUG with the divertor manipulator and the magnetic field lines is shown in Fig. 2. The H-mode series consisted of 8 identical consecutive discharges (AUG discharges #41467–74) with 6.2 MW of neutral beam heating (NBI) and 4.3 MW of electron cyclotron resonance heating (ECRH) whereas in the L-mode series with 6 discharges (AUG shots #41466, #41475–78, and #41480), only ECRH with a power of ~ 1 MW was used. To distinguish the erosion effect between L-mode and H-mode, the outer strike point (OSP) was moved on purpose poloidally by several centimeters. The residence time of OSP on the sample tiles during both the L- and H-mode phases is shown in Fig. 3 as a function of the poloidal S coordinate along the divertor surface. The integrated divertor plasma time was ~ 34 s for the L-mode series and ~ 41 s for the H-mode series.

The electron temperature measured by Langmuir probes was > 20 eV

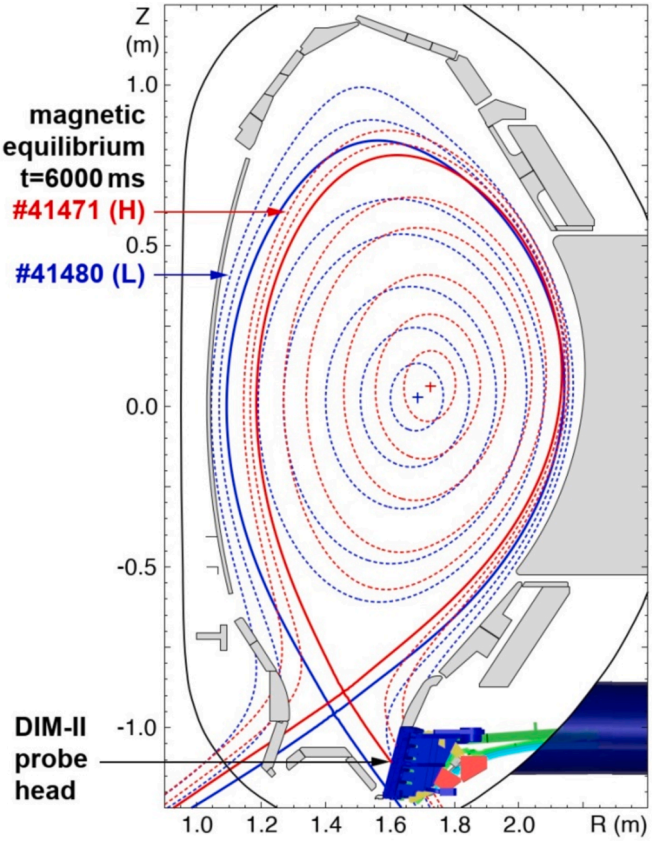

Fig. 2. Cross-section of AUG with the divertor manipulator and the equilibria of L-mode and H-mode scenario in the flat-top diverted plasma phase.

around the strike point both in the L-mode and H-mode (inter-ELM) phase. The plasma conditions of the experiment were as similar as possible to the 2019 He plasma experiments and the typical electron temperature profiles for the 2019 experiments are presented for example in ref. [18]. The accumulated particle fluence in the H-mode plasmas (see Fig. 3) reached a maximum of 3.4 × 10^{24} m^{-2} close to the strike point with a shallow decrease towards the scrape-off layer (SOL), while in the L-mode series the fluence was a factor ~ 10 smaller.

2.3. Post-exposure analysis

The erosion of the Pt marker layers was quantified by ion beam analysis at the accelerator laboratories of IPP Garching and RBI Zagreb. Rutherford backscattering spectroscopy (RBS) with 2.4 MeV ^{3}He ions was used for the 5 × 5 mm^2 Pt marker spots with the measured RBS

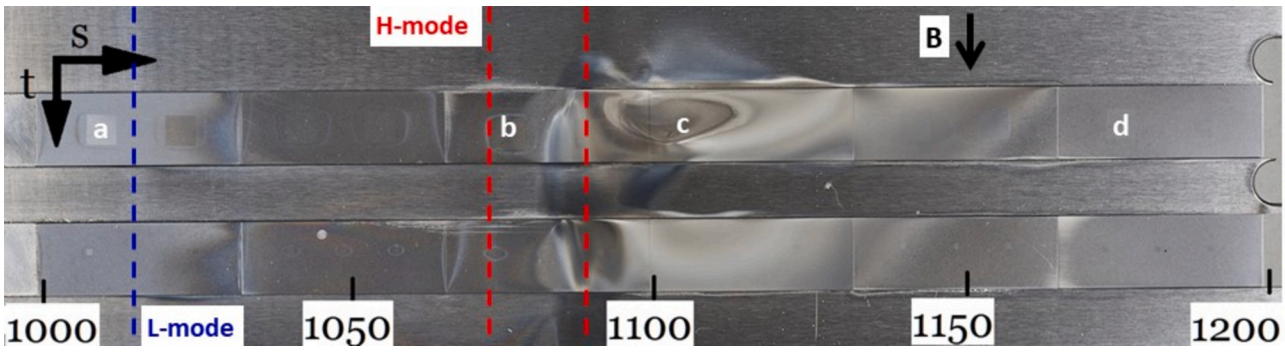

Fig. 1. Photo of the samples mounted on the DIM-II divertor manipulator target tile after exposure in ASDEX Upgrade. The main residence points of the strike lines of L-mode and H-mode plasmas are represented by the dashed lines and the residence time can be seen in more detail in Fig. 3.

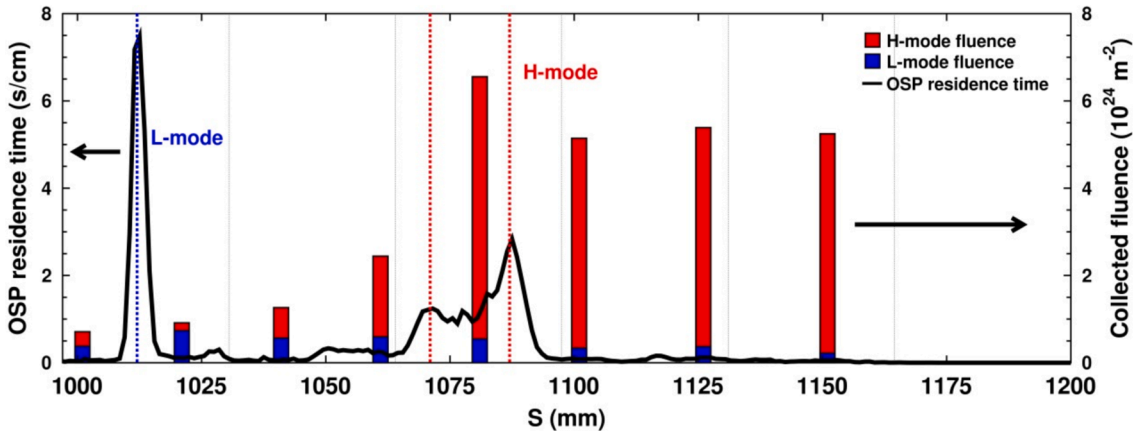

Fig. 3. Residence time of the outer strike point (black line and left y-axis) at specific areas of the divertor during plasma operation and the total particle fluence to the divertor on the right axis measured by Langmuir probes for the L-mode (blue bars) and H-mode (red bars). The dashed lines show the peak locations of residence time and correspond to those shown in Fig. 1 and other figures. (For interpretation of the references to colour in this figure legend, the reader is referred to the web version of this article.)

spectra quantitatively analyzed by the SIMNRA software [19].

Since RBS does not have sufficient energy resolution to distinguish high-Z elements with small relative mass differences, the areal densities of W and Pt in mixed layers were instead quantified by proton induced X-ray emission (PIXE) analysis using 1.5 MeV protons. In the measured X-ray spectra, the characteristic lines emitted from the L inner shell level transitions were used: at energies of 9.44 keV ($L\alpha_1$), 11.07 keV ($L\beta_1$), and 12.94 keV ($L\gamma_1$) for Pt, and 8.40 keV ($L\alpha_1$) for W. The respective areal densities were determined by comparing the peak intensities with those of unexposed reference samples. For Pt, the average of the three peaks was taken to improve accuracy.

MicroPIXE measurements for the 1 × 1 mm^2 Pt markers were performed using 2 MeV protons which were focused to an area of ~ 3 × 3 μm^2 and scanned across the marker over a central square area of ~ 700 × 700 μm^2.

Time-of-flight elastic recoil detection analysis (ToF-ERDA) measurements were performed for the 5 × 5 mm^2 Pt marker samples using 23 MeV $^{127}I^{7+}$ ions with an incidence angle of 20° towards the sample surface and a beam spot area of approximately 4 × 2 mm^2. Measurements were done both on and between the marker spots to quantify the D, He, and B areal densities.

The surface topography and local elemental composition were determined by scanning electron microscopy (SEM) and energy dispersive X-ray spectroscopy (EDX) in two microscopes with integrated EDX system at IPP Garching.

3. Results and discussion

3.1. Erosion and deposition of 5 × 5 mm^2 Pt markers

Substantial erosion is measured on all the 5 × 5 mm^2 Pt markers after exposure to H-mode plasma discharges. The maximum Pt erosion coincides with the strike point, as consistently observed in all erosion studies at AUG [8]. However, in contrast to D plasmas [14], the erosion profile remains at a comparatively high level towards the far SOL, which requires future interpretative modelling to identify the responsible processes. At several marker spots in locations close to the H-mode strike line, the original Pt layer was almost completely eroded. This can be seen in Fig. 4 where the RBS and PIXE results for the thickness of the marker spots after the experiment are plotted together with the values

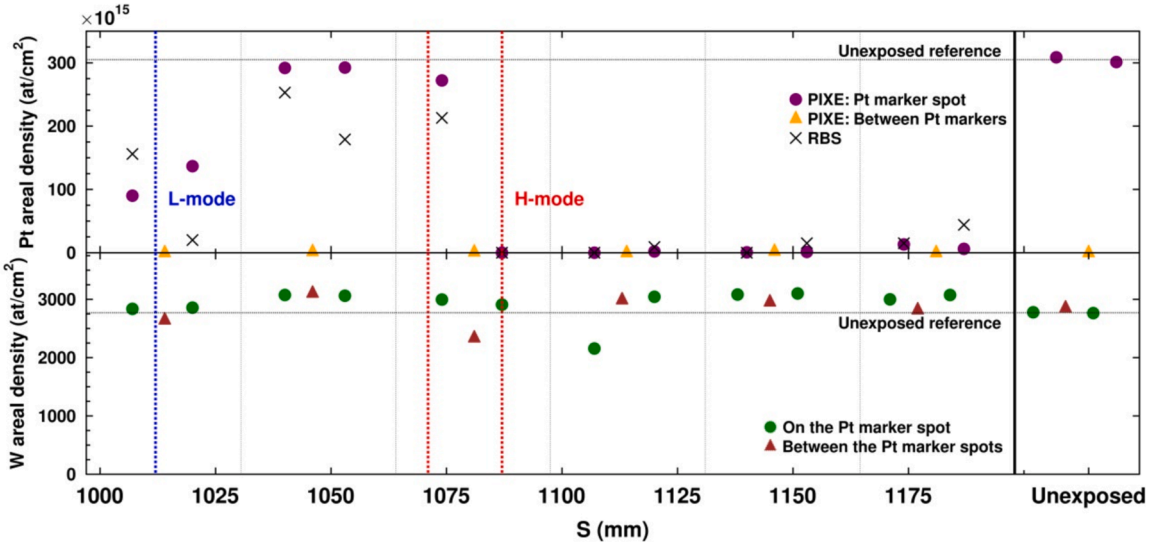

Fig. 4. Pt (top) and W (bottom) areal densities (at/cm^2) on the 5 × 5 mm^2 marker samples after plasma exposure measured by PIXE and RBS. Measurements have been made on both marker tile spots and between the spots. The reference PIXE measurement without plasma exposure is shown on the right. The measured PIXE data has been normalized to the RBS data of unexposed Pt samples.

for an unexposed reference marker. Due to the almost complete erosion of the Pt markers and significant material mixing with the underlying W layer, only a lower limit of 1.1 nm/s can be given for the Pt net-erosion rate during the H-mode experiment; in reality much higher net erosion rates are to be expected. The higher erosion by He plasma can be attributed to both the increased He impact energy due to sheath acceleration as a significant fraction of He^{2+} ions are present in the divertor SOL plasma in addition to the He^{+} ions [18] and the lower threshold energy and higher yield of Pt sputtering by He [20]. The calculated sputter yields for thermal plasma as a function of electron temperature T_e are presented in Fig. 5. The yields were computed by integrating the sputter yield as function of projectile (D or He) energy plus sheath energy gain (3 × Z × Te) over the Maxwellian distribution. The He sputtering yield is shown for He^{2+} ions which represent the main He ion fraction in the divertor under the conditions of this experiment [18]. The sputter yield in the figure shows the high difference between He^{2+} and D^{+} ions for both W and Pt. However, the sputtering curve shape and threshold energy for Pt and W by He^{2+} is comparable. Pt is sputtered about 4–5 times more efficiently but the effect is very similar otherwise. This means that Pt does work well as a proxy material for W in He plasma experiments. He can cause erosion to both W and Pt with the given plasma conditions unlike with D plasmas where the impurities dominate the PFM erosion.

In Fig. 4, the area between the L-mode and H-mode strike points showed the lowest Pt net erosion up to the point where changes in Pt marker thickness were below the detection threshold. As this area was exposed to the private flux region of the H-mode strike point, it is indeed an area of net deposition as discussed below for the ToF ERDA data. Subsequent exposure of this area to the L-mode plasma also did not result in any significant erosion, but in contrast to similar studies in D plasmas [14], no net deposition is observed. This suggests that the L-mode He plasma has eroded some of the previously deposited layers but not enough to erode the underlying Pt layer. Around the L-mode strike point, approximately 35 nm of the Pt layer has been eroded. This corresponds to a net erosion rate in the L-mode plasma of about 1.0 nm/s which is again higher than in D plasmas where erosion is also more concentrated around the strike point [14]. However, the deposition to this region caused by the previous H-mode discharges may have formed a layer on top of the Pt layer which had to be eroded first in the L-mode discharges before the Pt layer could be eroded. Therefore, the 1.0 nm/s value again represents only a lower limit for the Pt net erosion rate.

The PIXE signal at the Pt peak energy is at the background level in the area between the marker spots in Fig. 4, i.e. there is no detectable redeposition of Pt from the marker layers outside the marker area. In contrast, material migration simulations predict local redeposition adjacent to the marker spots, in both the toroidal and poloidal directions, resulting from combined prompt redeposition, local plasma transport and $\boldsymbol{E} \times \boldsymbol{B}$ drift [13,22]. The measured central point in between the markers is likely too far away from the marker areas so that the resulting Pt deposition is below the detection limit of the measurements. Although the experimental analysis is not sensitive enough to either verify or disprove the local deposition pattern of the simulations, campaign-integrated erosion data show many similarities between the modelled profiles [23].

The W areal density from the underlying W layer measured by PIXE is shown in the lower part of Fig. 4. The layer is mostly intact except for a few areas around the H-mode strike point. Some surface W and C deposition was observed on most of the samples by SEM-EDX (see images in Fig. 6). As AUG is a full W machine with W-coated graphite tiles, these elements are always present as residual plasma impurities and are therefore deposited in small amounts on the divertor target plates. In the most heavily eroded region outwards of the outer strike line, the Pt layer has been completely removed and even the underlying W coating on the tile has been deformed as seen in Fig. 6 (c) showing respective nanoscale features. This is similar to the pre-fuzz formation that has been observed on W samples exposed to He-plasmas [24]. The deposition of C and other impurities covers the W layer, shielding it from further plasma exposure. This mechanism has also been observed in previous He plasma operations [25].

The retention of He and the deposition of residual D and boron (B) are shown in Fig. 7 as measured by ToF-ERDA. Residual D impurities originate from previous D plasma operations and B from previous boronization. D retention is therefore quite low and is below 2.0×10^{16} D/cm^2 in all measured locations on the tile. The highest impurity deposition is observed in between the L-mode and H-mode strike points in the H-mode private flux region which is also the region with the lowest observed net erosion. The highest measured areal densities are 2.4×10^{17} B/cm^2 and 8.9×10^{16} He/cm^2. The deposits around the highly eroded H-mode strike point and on the SOL side of the strike point

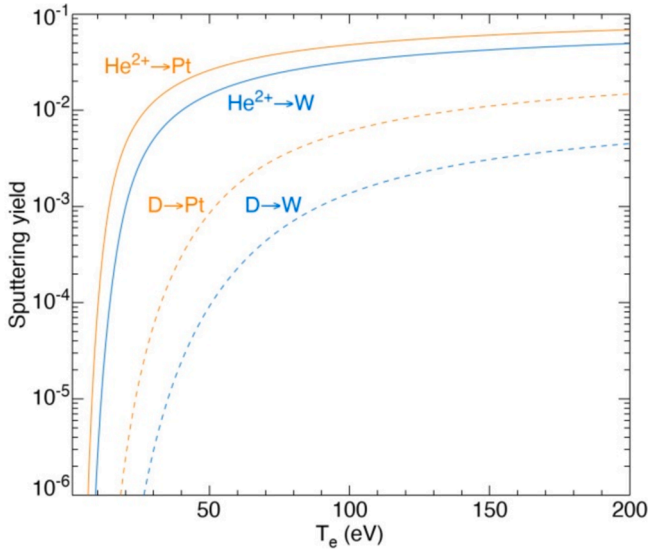

Fig. 5. Sputter yields for D^{+} and He^{2+} in W and in Pt as a function of electron temperature. The sputtering yields are calculated by using data from ref. [21].

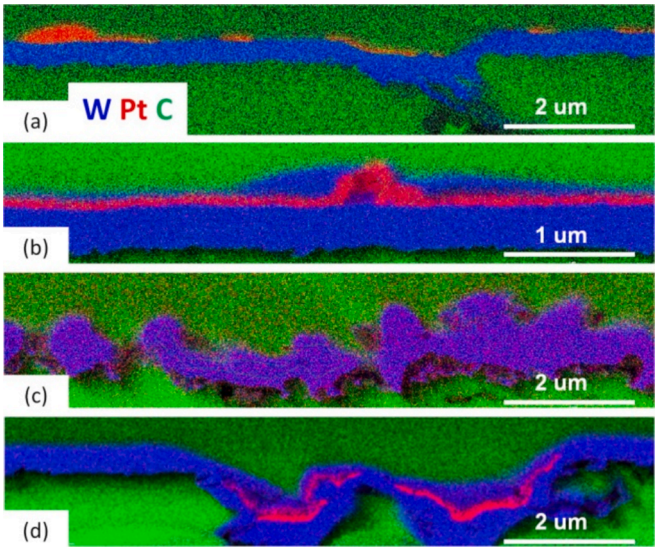

Fig. 6. SEM-EDX images of 5 × 5 mm^2 marker spots at locations with S coordinates of (a) 1008 mm, (b) 1074 mm, (c) 1108 mm, and (d) 1174 mm, which are also shown in Fig. 1. Image (a) shows partial erosion of the Pt layer, image (b) shows typical deposition on the Pt layer, in image (c) only a deformed W layer without Pt is visible, and in image (d), the Pt layer has been mostly eroded and only traces of Pt remained in grooves together with W deposition. The pure C layer on top of the W and Pt layers was deposited as protective cover for focused ion beam cutting of the samples.

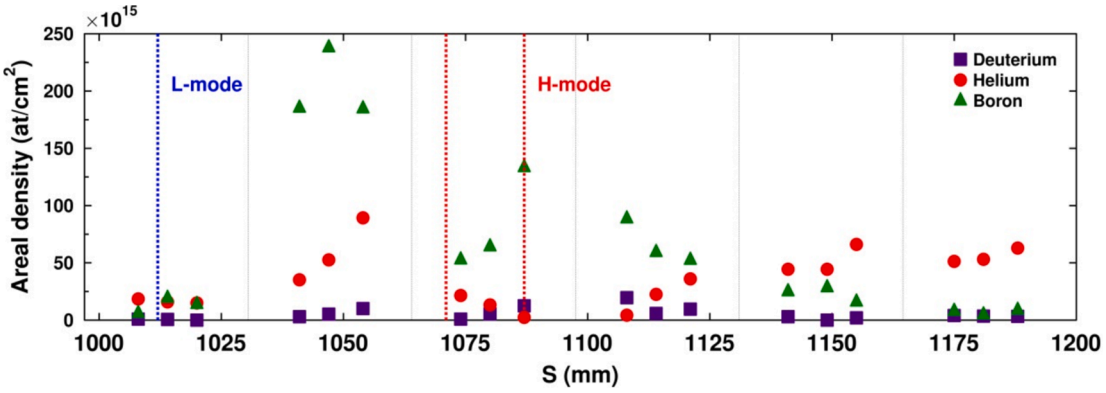

Fig. 7. ToF-ERDA measurement data of the 5 × 5 mm^2 sample areal densities of D, He, and B on the Pt marker spots and in between the markers. The amount of B on the S coordinates of 1087 mm and 1108 mm may be slightly overestimated due to background counts coming from the C region in the ToF-ERDA data.

may be due to the previously mentioned $\boldsymbol{E} \times \boldsymbol{B}$ drift during the L-mode discharges that followed the H-mode part of the experiment. Significant He implantation has been observed in the area exposed to the far SOL plasma as areal densities up to 6.6 × 10^{16} He/cm^2 are measured. This He retention is similar to the observations in the previous H-mode He plasma experiments on AUG [25]. Further into the SOL the He inventories appear to increase gradually. In the region close to the strike line, the He retention is much lower and stays below 2.2 × 10^{16} He/cm^2 despite the higher incident fluence. This can be explained by the much higher sample temperature due to the power flux maximum in this region and to some extent also by high (re-)erosion of both the deposited impurities and the underlying sample. Very little He and impurity deposition is measured also close to the L-mode strike point where both He and B are below 2.0 × 10^{16} at./cm^2. In comparison to [25], no boronization was performed prior to the experiment, which reduces the amount of B and other impurities present in the SOL plasma.

3.2. Erosion of 1 × 1 mm^2 Pt markers

The areal density of the remaining Pt and the deposited amount of W on the smaller 1 × 1 mm^2 Pt marker samples are shown in Fig. 8. The Pt erosion on the markers mostly follows the same trend as for the 5 × 5 mm^2 Pt markers in Fig. 4. Due to the complete erosion of the markers in the area exposed to the H-mode plasma, no effects of marker size can be seen there. However, in the region exposed to the L-mode plasma, the small markers show significantly higher erosion than the large markers although they received ~ 30 % lower plasma fluence because of the decreasing *B*-field intersection angle with the tile surface and the 22 mm toroidal distance between the large and small marker samples. This suggests that, in line with the impurity transport modelling, Pt is indeed locally redeposited, which manifests itself as a lower net erosion compared to the small markers where local Pt redeposition is negligible and the observed Pt erosion therefore corresponds to the gross erosion rate.

The same mechanism manifests itself also in the W areal density on the small markers (Fig. 8), which is significantly higher than on the 5 × 5 mm^2 markers shown in Fig. 4. This is particularly the case around the H-mode strike line, where the 1 × 1 mm^2 markers show W deposition of around 9 × 10^{17} W/cm^2, whereas the corresponding 5 × 5 mm^2 markers show no significant W deposition. These results suggest that prompt redeposition of W eroded adjacent to the Pt markers could occur on the small marker spots, whereas on the large marker spots, prompt

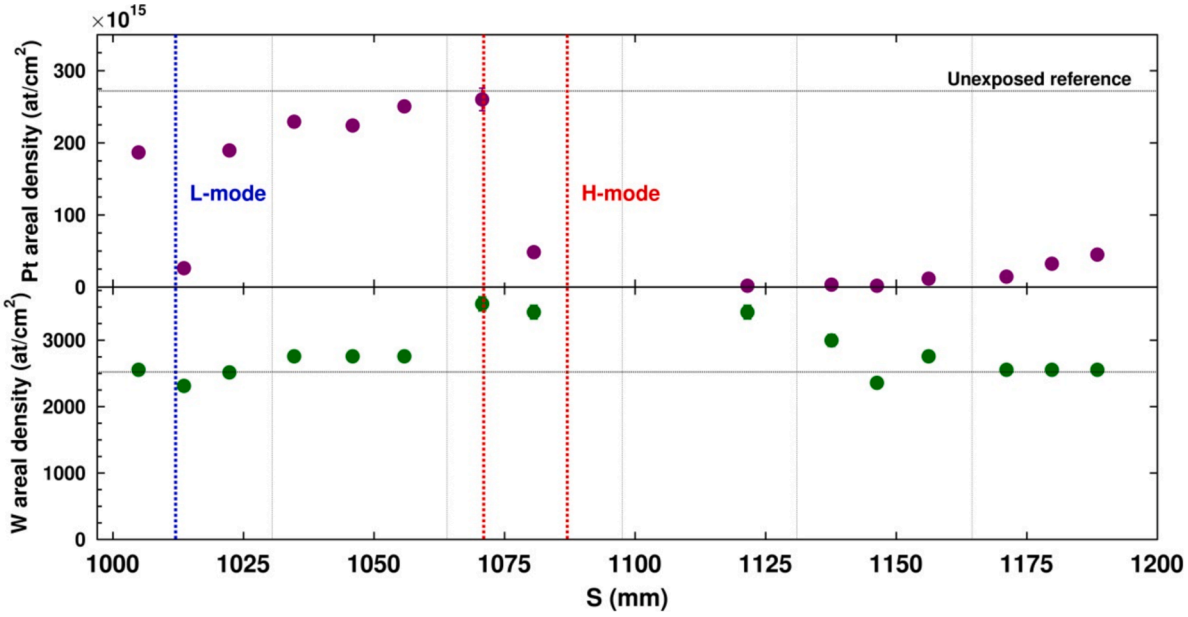

Fig. 8. Pt (top, purple dots) and W (bottom, green dots) areal densities of the 1 × 1 mm^2 Pt marker samples as measured by microPIXE. The unexposed reference lines correspond to samples without plasma exposure. (For interpretation of the references to colour in this figure legend, the reader is referred to the web version of this article.)

redeposition of W would not extend to the center of the marker where the RBS and PIXE analyses were performed. Further measurements of the erosion/deposition profiles across the large markers by microbeam analysis will be required to validate this interpretation.

4. Conclusions

Erosion measurements on Pt marker samples exposed in dedicated L-mode and H-mode discharges in the outer divertor of ASDEX Upgrade confirmed the higher erosion rates under He plasma exposure compared to D plasmas, as expected from the higher sputtering yield of He and its lower sputtering threshold energy. The radial profile of Pt erosion in He also extended further out in the poloidal direction compared to D plasmas where the erosion is much more localized in the strike point zone. No redeposited Pt was detected in the vicinity of the large Pt marker spots, suggesting that any redeposition of Pt is strongly localized within the marker spots whereas for the small markers the total amount of redeposited Pt in the vicinity of the marker area is likely to be below the detection threshold. The Pt can work as a proxy for W due to similar shape of the sputtering yield curves and therefore the results can be applied to W surfaces, although the erosion is stronger with Pt surfaces. But with both Pt and W, the He plasma itself is the main factor for the erosion unlike with D plasmas where the impurities within the plasma dominate the erosion behavior.

Deposition of residual D and B was observed in the private flux region of the H-mode plasma in between the H-mode and L-mode strike points. The subsequent L-mode discharges were not sufficient to induce significant erosion in this region. He retention differed from that of residual D and B, showing an increase further out from the strike point area, with the lower retention values near the OSP attributed mostly to the higher surface temperatures reached in this region during plasma exposure.

CRediT authorship contribution statement

Tomi Vuoriheimo: Writing – original draft, Visualization, Investigation, Formal analysis. **Antti Hakola:** Writing – review & editing, Writing – original draft, Supervision, Project administration, Conceptualization. **Jari Likonen:** Project administration, Conceptualization. **Karl Krieger:** Writing – review & editing, Validation, Supervision, Resources, Investigation. **Martin Balden:** Writing – review & editing, Validation, Resources, Investigation, Formal analysis, Data curation. **Iva Bogdanović Radović:** Writing – review & editing, Validation, Formal analysis. **Georgios Provatas:** Investigation, Formal analysis. **Zdravko Siketić:** Investigation. **Karla Ivanković Nizić:** Investigation, Formal analysis. **Marcin Rasinski:** Investigation. **Sebastijan Brezinsek:** Project administration.

Declaration of competing interest

The authors declare that they have no known competing financial interests or personal relationships that could have appeared to influence the work reported in this paper.

Acknowledgements

This work has been carried out within the framework of the EUROfusion Consortium, funded by the European Union via the Euratom Research and Training Programme (Grant Agreement No 101052200 — EUROfusion). Views and opinions expressed are however those of the author(s) only and do not necessarily reflect those of the European Union or the European Commission. Neither the European Union nor the European Commission can be held responsible for them.

Open access funded by Helsinki University Library

Data availability

Data will be made available on request.

References

[1] R. Pitts, S. Carpentier, F. Escourbiac, T. Hirai, V. Komarov, S. Lisgo, A. S. Kukushkin, A. Loarte, M. Merola, A. Sashala Naik, R. Mitteau, M. Sugihara, B. Bazylev, P.C. Stangeby, A full tungsten divertor for ITER: Physics issues and design status, J. Nucl. Mater. 438 (2013) S48–S56, https://doi.org/10.1016/j.jnucmat.2013.01.008.

[2] R. Pitts et al., Plasma-wall interaction impact of the ITER re-baseline, Submitt. to Nucl. Mater. Energy. (2024).

[3] J.H. You, E. Visca, C. Bachmann, T. Barrett, F. Crescenzi, M. Fursdon, H. Greuner, D. Guilhem, P. Languille, M. Li, S. McIntosh, A.V. Müller, J. Reiser, M. Richou, M. Rieth, European DEMO divertor target: Operational requirements and material-design interface, Nucl. Mater. Energy. 9 (2016) 171–176, https://doi.org/10.1016/J.NME.2016.02.005.

[4] S. Brezinsek, A. Kirschner, M. Mayer, A. Baron-Wiechec, I. Borodkina, D. Borodin, I. Coffey, J. Coenen, N. den Harder, A. Eksaeva, C. Guillemaut, K. Heinola, A. Huber, V. Huber, M. Imrisek, S. Jachmich, E. Pawelec, M. Rubel, S. Krat, G. Sergienko, G.F. Matthews, A.G. Meigs, S. Wiesen, A. Widdowson, J.E.T. contributors, Erosion, screening, and migration of tungsten in the JET divertor, Nucl. Fusion. 59 (2019) 96035, https://doi.org/10.1088/1741-4326/ab2aef.

[5] M. Balden, M. Mayer, B. Bliewert, E. Bernard, M. Diez, M. Firdaouss, M. Missirlian, B. Pégourié, M. Richou, H. Roche, E. Tsitrone, C. Martin, A. Hakola, the WEST Team, Erosion and redeposition patterns on entire erosion marker tiles after exposure in the first operation phase of WEST, Phys. Scr. 96 (2021) 124020, https://doi.org/10.1088/1402-4896/ac2182.

[6] F. Ding, G.-N. Luo, X. Chen, H. Xie, R. Ding, C. Sang, H. Mao, Z. Hu, J. Wu, Z. Sun, L. Wang, Y. Sun, J. Hu, the E. Team, Plasma–tungsten interactions in experimental advanced superconducting tokamak (EAST), Tungsten. 1 (2019) 122–131. 10.1007/s42864-019-00019-4.

[7] H. Xie, R. Ding, A. Kirschner, J.L. Chen, F. Ding, H.M. Mao, W. Feng, D. Borodin, L. Wang, ERO modelling of tungsten erosion and re-deposition in EAST L mode discharges, Phys. Plasmas. 24 (2017) 92512, https://doi.org/10.1063/1.4991457.

[8] A. Hakola, J. Likonen, A. Lahtinen, T. Vuoriheimo, M. Groth, H. Kumpulainen, M. Balden, K. Krieger, M. Mayer, T. Schwarz-Selinger, S. Brezinsek, M. Kelemen, S. Markelj, M. Barac, S. Gouasmia, I. Bogdanovic Radovic, A. Uccello, E. Vassallo, D. Dellasega, M. Passoni, M. Sala, E. Bernard, M. Diez, C. Guillemaut, E., Tsitrone, the ASDEX Upgrade Team, the EUROfusion MST1 Team, the EUROfusion WP PFC Contributors, Gross and net erosion balance of plasma-facing materials in full-W tokamaks, Nucl. Fusion. 61 (2021) 116006, https://doi.org/10.1088/1741-4326/ac22d2.

[9] S. Kajita, W. Sakaguchi, N. Ohno, N. Yoshida, T. Saeki, Formation process of tungsten nanostructure by the exposure to helium plasma under fusion relevant plasma conditions, Nucl. Fusion. 49 (2009) 95005, https://doi.org/10.1088/0029-5515/49/9/095005.

[10] Y. Ueda, H.Y. Peng, H.T. Lee, N. Ohno, S. Kajita, N. Yoshida, R. Doerner, G. De Temmerman, V. Alimov, G. Wright, Helium effects on tungsten surface morphology and deuterium retention, J. Nucl. Mater. 442 (2013) S267–S272, https://doi.org/10.1016/J.JNUCMAT.2012.10.023.

[11] S. Brezinsek, A. Hakola, H. Greuner, M. Balden, A. Kallenbach, M. Oberkofler, G. De Temmerman, D. Douai, A. Lahtinen, B. Böswirth, D. Brida, R. Caniello, D. Carralero, S. Elgeti, K. Krieger, H. Mayer, G. Meisl, S. Potzel, V. Rohde, B. Sieglin, A. Terra, R. Neu, C. Linsmeier, Surface modification of He pre-exposed tungsten samples by He plasma impact in the divertor manipulator of ASDEX Upgrade, Nucl. Mater. Energy. 12 (2017) 575–581, https://doi.org/10.1016/J.NME.2016.11.002.

[12] A. Hakola, M.I. Airila, J. Karhunen, M. Groth, A. Herrmann, K. Krieger, T. Kurki-Suonio, G. Meisl, M. Oberkofler, R. Neu, S. Potzel, V. Rohde, and the ASDEX Upgrade Team, Gross and net erosion of tungsten in the outer strike-point region of ASDEX Upgrade, Phys. Scr. (2016) 14026, https://doi.org/10.1088/0031-8949/T167/1/014026.

[13] A. Hakola, A. Keitaanranta, H. Kumpulainen, A. Lahtinen, J. Likonen, M. Balden, M. Cavedon, K. Krieger, M. Airila, M. Groth, ERO modelling of net and gross erosion of marker samples exposed to L-mode plasmas on ASDEX Upgrade, Nucl. Mater. Energy. 25 (2020) 100863, https://doi.org/10.1016/J.NME.2020.100863.

[14] A. Lahtinen, A. Hakola, J. Likonen, M. Balden, K. Krieger, S. Gouasmia, I. Bogdanovic Radovic, G. Provatas, M. Kelemen, S. Markelj, M. Pedroni, A. Uccello, E. Vassallo, D. Dellasega, M. Passoni, Influence of surface morphology on erosion of plasma-facing components in H-mode plasmas of ASDEX Upgrade, Nucl. Mater. Energy. 33 (2022) 101266, https://doi.org/10.1016/J.NME.2022.101266.

[15] A. Herrmann, N. Jaksic, P. Leitenstern, H. Greuner, K. Krieger, P. De Marné, M. Oberkofler, V. Rohde, G. Schall, A large divertor manipulator for ASDEX Upgrade, Fusion Eng. Des. 98–99 (2015) 1496–1499, https://doi.org/10.1016/J.FUSENGDES.2015.02.007.

[16] M. Rasiński, S. Brezinsek, A. Kreter, T. Dittmar, K. Krieger, M. Balden, P. de Marne, R. Dux, M. Faitsch, A. Hakola, J. Likonen, E. Tsitrone, V. Rohde, FIB line marking as a tool for local erosion/deposition/fuzz formation measurements in ASDEX Upgrade during the He campaign, Nucl. Mater. Energy. 37 (2023) 101539, https://doi.org/10.1016/J.NME.2023.101539.

[17] A. Hakola, M. Balden, M. Baruzzo, R. Bisson, S. Brezinsek, T. Dittmar, D. Douai, M. Dunne, L. Garzotti, M. Groth, R. Henriques, L. Horvath, I. Jepu, E. Joffrin, A. Kappatou, D. Keeling, K. Krieger, B. Labit, M. Lennholm, J. Likonen, A. Loarte, P. Lomas, C. Lowry, M. Maslov, D. Matveev, R.A. Pitts, U. Plank, M. Rasinski, D. Ryan, S. Saarelma, S. Silburn, E.R. Solano, W. Suttrop, T. Tala, E. Tsitrone, N. Vianello, T. Wauters, A. Widdowson, M. Wischmeier, the Euro.T. Exploitation Team, the A.U. Team, J.E.T. Contributors, Helium plasma operations on ASDEX Upgrade and JET in support of the non-nuclear phases of ITER, Nucl. Fusion. 64 (2024) 96022. 10.1088/1741-4326/ad6335.

[18] E. Tonello, Modelling of boundary plasmas in linear devices and tokamaks, Politecnico di Milano, 2023. https://hdl.handle.net/10589/196383.

[19] M. Mayer, SIMNRA 7.03, (2020). https://mam.home.ipp.mpg.de/.

[20] G.H. Al-Malkawi, A.M.B.A. Al-Ajlony, K.f. AL-Shboul, Computer simulation of the sputtering energy thresholds for some plasma-facing component materials irradiated with helium, deuterium, and tritium ions, Nucl. Mater. Energy. 35 (2023) 101442, https://doi.org/10.1016/J.NME.2023.101442.

[21] W. Eckstein, C. Garcia-Rosales, J. Roth, W. Ottenberger, Sputtering data, 1993. http://cds.cern.ch/record/832227.

[22] L. Aho-Mantila, M. Wischmeier, K. Krieger, V. Rohde, A. Hakola, S. Potzel, A. Kirschner, D. Borodin, The ASDEX Upgrade Team, Outer divertor of ASDEX Upgrade in low-density L-mode discharges in forward and reversed magnetic field: II. Analysis of local impurity migration, Nucl. Fusion. 52 (2012) 103007, https://doi.org/10.1088/0029-5515/52/10/103007.

[23] M. Mayer, M. Andrzejczuk, R. Dux, E. Fortuna-Zalesna, A. Hakola, S. Koivuranta, K. Krieger, K.J. Kurzydlowski, J. Likonen, G. Matern, R. Neu, G. Ramos, M. Rasinski, V. Rohde, K. Sugiyama, A. Wiltner, W. Zielinski, A.-u. Team, Tungsten erosion and redeposition in the all-tungsten divertor of ASDEX Upgrade, Phys. Scr. (2009) 14039, https://doi.org/10.1088/0031-8949/2009/T138/014039.

[24] P. Fiflis, D. Curreli, D.N. Ruzic, Direct time-resolved observation of tungsten nanostructured growth due to helium plasma exposure, Nucl. Fusion. 55 (2015) 33020, https://doi.org/10.1088/0029-5515/55/3/033020.

[25] A. Hakola, S. Brezinsek, D. Douai, M. Balden, V. Bobkov, D. Carralero, H. Greuner, S. Elgeti, A. Kallenbach, K. Krieger, G. Meisl, M. Oberkofler, V. Rohde, P. Schneider, T. Schwarz-Selinger, A. Lahtinen, G. De Temmerman, R. Caniello, F. Ghezzi, T. Wauters, A. Garcia-Carrasco, P. Petersson, I.B. Radovic, Z. Siketic, A.U. Team, Euro.M. Team, Plasma-wall interaction studies in the full-W ASDEX upgrade during helium plasma discharges, Nucl. Fusion. 57 (2017) 66015. 10.1088/1741-4326/aa69c4.